High Temperature Oxidation of Boron Nitride
Part I—Monolithic Boron Nitride

Nathan Jacobson and Serene Farmer
NASA Lewis Research Center
Cleveland, OH 44135

Arthur Moore and Haluk Sayir
Advanced Ceramics Corporation
Lakewood, OH

Abstract

High temperature oxidation of monolithic boron nitride (BN) is examined. Hot pressed BN and both low and high density CVD BN were studied. It is shown that oxidation rates are quite sensitive to microstructural factors such as orientation, porosity, and degree of crystallinity. In addition small amounts of water vapor lead to volatilization of the B_2O_3 oxide as $H_xB_yO_z$. For these reasons, very different oxidation kinetics were observed for each type of BN.

Introduction

Monolithic boron nitride has long been used as a crucible material in inert environments at high temperatures. Recently it has found application as a fiber coating in ceramic matrix composites. In such applications, it is likely to be exposed to high temperature oxidizing conditions. However, there are many questions about its oxidation behavior.

The literature indicates that the oxidation behavior of BN is complex and highly dependent on structure. BN is an analog of graphite and occurs in several crystalline forms (1).

α–BN—Hexagonal structure, similar to graphite.
β–BN—Diamond-like structure.
γ–BN—Wurtzite structure.

In addition, α–BN can form with turbostratic defects, i.e. rotational stacking disorder from plane to plane. In general, higher temperature synthesis routes lead to more crystalline BN.

The literature contains numerous studies of BN oxidation (2-11). Many different rates and rate laws have been reported and there is no agreement on the fundamental mechanism of oxidation. These varying results suggest that

oxidation behavior is dependent on issues such as porosity, additives, and crystalline form.

Oda and Yoshio (7) have examined α–BN powder oxidation. They observe linear kinetics and apply a shrinking sphere model. They also observe weight losses, which are suppressed in air as opposed to oxygen. Microstructure observations of the individual grains indicate that the rate of attack was dependent on crystallographic orientation. Initially the grains of BN have a round, plate-like shape. After oxidation and removal of the B_2O_3 film with water, the remaining BN grains are smaller along the a-axis. This suggests the c-axis is much less reactive, which is analogous to graphite and consistent with the weaker bonding between hexagonal planes.

Lavrenko and Alexeev (8) have examined a series of α–BN and γ–BN powder compacts. Their α–BN, which has a large degree of disorder, exhibits only weight losses at 900-1200°C. However the more graphitic α–BN, which possesses a more ordered structure, gains weight over this temperature range with generally linear kinetics. γ–BN exhibits parabolic kinetics at 900, 1000 and 1100°C. At 1200°C there is a linear weight loss component.

It is well-known that BN is highly sensitive to water vapor. Coffer and Economy (9) have examined a series of BN powders with different interplanar [d(002)] spacings between 3.33 and 3.67 angstroms. The samples with larger interplanar spacings exhibited greater weight loss in a stream of H_2O/air and H_2O/N_2 at 700°C. Mass spectrometry indicated that the primary volatile product was HBO_2 with smaller amounts of H_3BO_3. In dry air, weight increases were observed, which again were dependent on the interplanar spacings, with the larger spacings producing more weight gain.

Similar effects have been observed by other investigators. Matsuda (10) has studied the effects of moisture on CVD BN, synthesized from $BCl_3 + NH_3 + H_2$. As prepared specimens were compared to those aged at room temperature for 60 days with 65-80% relative humidity. It was found that specimens synthesized at 2000°C showed better moisture resistance than those synthesized at 1400°C. The lower temperature materials tended to form ammonium boron hydrates. At higher temperatures and in argon atmospheres, these decomposed leading to weight losses of about 20% from 200-400°C:

$$(NH_2)_2O.4B_2O_3 .6H_2O = 4\ B_2O_3 + 7\ H_2O + NH_3$$

$$(NH_2)_2O.4B_2O_3 .6H_2O = 5\ B_2O_3 + 9\ H_2O + 2\ NH_3$$

The correlation of increased moisture sensitivity with lower deposition temperature and hence lower crystallinity is consistent with other findings.

Part I of this paper is a fundamental oxidation study of pure BN. Particular attention is given to the structure/oxidation property correlations discussed above. Part II of this paper is a study of BN oxidation inside a silicon carbide (SiC) matrix.

Experimental

Starting Materials

Initial experiments were done using hot pressed (HP) BN*. This material consisted of randomly oriented crystallites. However, most of this study dealt with chemically-vapor-deposited (CVD) BN** in the form of flat plates. These were pyrolytic BN, deposited at high temperatures from BCl_3 and NH_3. Deposition temperatures ranged from ~1900°C to ~1400°C, with the higher temperatures giving a more dense and more crystalline structure. X-ray diffraction (XRD) results for the hot pressed and two CVD materials are shown in Figure 1. This figure shows the random orientation for the HP BN and the c-axis orientation for the CVD materials. The broader peaks for the low density CVD BN indicate less crystallinity as compared to the high density CVD BN.

Type of BN	Designation	Density—Water
Hot Pressed	HP BN	2.18
CVD—High density	High density CVD BN	2.12-2.19
CVD—Low density	Low density CVD BN	1.76
Theoretical		2.27

Table I. Measured densities of each type of BN studied in gm/cc.

Oxidation Studies

Oxidation studies were done in a thermogravimetric apparatus (TGA). The specimens were cut into coupons with dimensions approximately 3 cm x 1 cm x 1 cm and a hole for the hangwire. Samples were washed in a non-aqueous solvent (trichlorethane) and dried before each run. The sample was suspended from a sapphire fiber connected to a recording electrobalance*** . A quartz furnace tube was used with a molybdenum disilicide furnace. Data from the balance (weight gain vs. time) was collected on a computer for plotting and processing.

---

* Carborundum Co., Amherst, NY.

** Advanced Ceramics Corporation, Lakewood, OH.

*** Cahn Instruments, Cerritos, CA.

The moisture content of the gas stream was minimized and monitored. High purity oxygen (99.99 or 99.999%) was used and dried over a tower of $MgClO_2$ followed by P_2O_5. Clean stainless steel lines were used throughout. At the exit of the balance, a chilled-mirror hygrometer† was used to continuously monitor the dew-point. Although the water vapor content was constant during a run, there was variation from run to run. Nearly all runs had measured dew points between -50°C and -60°C (30-10 ppm water). There appeared to be some correlation with the quality of oxygen used.

Mass Spectrometry

As discussed in the introduction, volatile products are often encountered in the high temperature oxidation of BN. They were identified with a unique molecular beam mass spectrometer (MBMS), suitable for direct sampling of a 1 bar process. This instrument has been described elsewhere (11) and will only be briefly summarized here. It consists of a small (0.2 mm) orifice in a large, rapidly pumped vacuum chamber. This forms a free-jet expansion and a well-defined supersonic molecular beam. A series of differentially pumped vacuum chambers and collimators direct the beam into an ultra-high vacuum chamber with a quadrupole mass spectrometer††. This allows direct mass spectrometric identification of the volatile species, while preserving their chemical and dynamic integrity. Due the complexity of the free-jet expansion, it is not possible to convert ion-intensity measurements to absolute vapor pressures. However important qualitative trends can be observed.

Thermochemical Considerations

Like most nitrides, BN is thermochemically unstable relative to the corresponding oxide, B_2O_3. This oxide has an unusually low melting point of 410°C (12). The primary oxidation reaction is generally written:

$$2\ BN(s) + 3/2\ O_2(g) = B_2O_3(l) + N_2(g) \qquad (1)$$

It should be noted that $N_2(g)$ may also further oxidize to $NO_x(g)$. In pure oxygen, the vapor pressure of B_2O_3 is relatively low at 1000°C, as shown in Figure 2(a). This figure was calculated from a free-energy minimization (13) of B_2O_3 + 1 bar of oxygen. The products shown represent the minimium free energy for this assemblage of atoms under the constraints of constant pressure and mass. Although our actual experiment is an opened, flowing system, this calculation is a reasonable approximation. A small amount of water vapor creates numerous species at high vapor pressures, due to the extraordinary stability of $H_xB_yO_z(g)$ species. This is shown in Figure 2(b), which is the result of a free-energy

† General Eastern Instruments, Woburn, MA.
†† ABB Extrel, Pittsburgh, PA.

minimization of B_2O_3 + 1 bar of oxygen + 20 ppm H_2O. We found that below about 1100°C, only a small amount of the 20 ppm H_2O was consumed in the reaction. However above 1100°C most of the water vapor is consumed. This indicates that Figure 2(b) only models our flowing system with a constant pressure of water vapor at about 20 ppm at 1100°C and below.

Results and Discussion

I. Hot Pressed BN

A typical TGA trace for this type of BN at 900°C is shown in Figure 3. There appears to be a period of rapid weight gain and second region of linear weight gain. Note also that both rates are linear, indicating no protective film formation and that an interface reaction is very likely rate controlling. The second linear region indicates a decrease in reaction rates by about a factor of ten. Microstructural observations indicate that there are large regions of internal oxidation. It is likely that the reduced rates observed after about 15 hrs occurs when all the easily oxidizable grains are consumed.

A SEM photograph of this specimen is shown in Figure 4. Most of the surface is covered by solidified B_2O_3, however some BN grains remain at the surface, as the associated EDS traces show. This is likely due to an orientation effect. A close examination of the BN grain in the center of Figure 4 shows oxide growing on one edge, but not on the face, indicating preferential oxidation. Oda and Yoshio (7) have seen similar effects in their studies.

II. High Density CVD BN

This material has a highly oriented crystalline structure with near theoretical density. This material was oxidized at 900, 1000, 1100, and 1200°C. In most cases, paralinear kinetics were observed, which are a mixture of simultaneous parabolic and linear kinetics. Figure 5(a) and (b) are some representative TGA traces. In some cases, only parabolic behavior was observed. Table II summarizes this behavior.

Run	T (°C)	Dew Pt.	Parabolic/ Paralinear	k_p—Expt. (mg^2/cm^4-hr)	$-k_l$--Expt. (mg/cm^2-hr)	$-k_l$—Calc (mg/cm^2-hr)
BN305	900	-56.9	Paralinear	4.9×10^{-4}	5.4×10^{-3}	3.3×10^{-3}
BN306	900	-53.9	Paralinear	4.2×10^{-4}	6.4×10^{-3}	3.3×10^{-3}
BN307	1000	-57.3	Paralinear	3.6×10^{-3}	1.7×10^{-2}	1.2×10^{-2}
BN309	1000	-60.0	Paralinear	2.1×10^{-3}	1.7×10^{-2}	1.2×10^{-2}
BN302	1100	-60.0	Paralinear	1.6×10^{-2}	1.8×10^{-2}	2.9×10^{-2}
BN313	1100	-53.9	Paralinear	8.0×10^{-3}	2.4×10^{-2}	2.9×10^{-2}
SFBN3*	1100	-60.0	Paralinear	8.9×10^{-3}	3.5×10^{-2}	2.9×10^{-2}
BN311	1200	-48.4	Paralinear	4.5×10^{-2}	5.7×10^{-2}	
BN310	1200	-56.8	Paralinear	4.0×10^{-2}	6.4×10^{-2}	
BN203	900	-63.6	Parabolic	5.2×10^{-4}		
LSBN1	900	-61.5	Parabolic	2.1×10^{-4}		
SFBN5	1000	-61.1	Parabolic	2.0×10^{-3}		
LSBN2	1100	-61.2	Parabolic	2.1×10^{-2}		

Table II. Measured rates for CVD BN. All are in 100% oxygen, except SFBN3* which was in 10% H_2O/O_2.

Note that weight gains were much less than those measured for the hot pressed material. Figure 6 is an SEM photo of the surface after 50 hrs oxidation at 900°C. Both oxygen and nitrogen are present in EDS, indicating a thin layer of solidified B_2O_3.

We believe that the oxidation kinetics are always paralinear. As will be shown, the linear portion is likely due to water vapor interactions with the B_2O_3 scale to form $H_xB_yO_z(g)$ species. Local water vapor variations at the sample surface create more $H_xB_yO_z(g)$ and make the linear component more pronounced. These local variations may not be strongly reflected in the measured dew point of the exit stream.

Paralinear kinetics (15) are caused by simultaneous parabolic weight gain and linear weight loss. In terms of oxide scale thickness, paralinear kinetics (16) are described by:

$$\frac{dx}{dt} = \frac{k_p}{x} - k_l \tag{2}$$

This can be integrated to:

$$t = \frac{k_p}{2k_l}\left[\frac{2k_l x}{k_p} - \ln\left(1 - \frac{2k_l x}{k_p}\right)\right] \tag{3}$$

and can be converted from thickness changes to weight changes by:

$$x = \frac{\Delta M / A}{\alpha \rho_{oxide}}$$
$$t = \frac{\beta^2 k_p}{2\alpha^2 k_{li}^2}\left[\frac{-2\alpha k_{li}(\Delta M/A)}{\beta k_p} - \ln\left(1 - \frac{2\alpha k_{li}(\Delta M/A)}{\beta k_p}\right)\right] \quad (4)$$

where:

$$a = \frac{MW_{O_2} - MW_N}{MW_{B_2O_3}}$$
$$\beta = \frac{MW_{O_2}}{MW_{B_2O_3}} \quad (5)$$

The α and β terms are included since reaction (1) generates both condensed and volatile products.

In order to illustrate the influence of k_p and k_l on the overall kinetics, several simulations were run as shown in Figure 7(a) and (b). Both are paralinear, but the paralinear behavior would not be evident in the second curve in a short term run. This explains why in some cases "parabolic" behavior was observed.

Recently, Opila and Hann (17) have developed a non-linear least squares computer code which fits the data to a paralinear curve and extracts a linear and parabolic rate constant. The generated curve is the solid line in Figure 5(b). This close fit of the generated paralinear curve to the experimental measurements was typical of each of the four temperatures studied. Table III lists the parabolic rate and linear rate constants extracted from these paralinear test results. Also listed are the parabolic rate constants from the runs which did not exhibit a linear component. Note the similarity of these parabolic rate constants to those extracted from the paralinear curves. This confirming the validity of the approach.

Let us consider the linear component in detail. As previously noted, the linear portion is likely due to water vapor interactions with the B_2O_3 scale to form $H_xB_yO_z(g)$ species. In order to show these species are generated, we looked for the volatile species with our MBMS system. Much larger amounts of water vapor were used (~2% H_2O/O_2) in order to observe the vapor species. Table III lists the intensities of the principle peaks. Locating peaks between about 12 to 20 m/e ratio and 28 to 34 m/e was very difficult due to the large amounts of oxygen in the gas stream and water vapor and nitrogen from the vacuum chamber.

These tended to mask the signals coming off the sample. However, there is clear evidence for $HBO_2(g)$, $H_3BO_3(g)$, and $NO_2(g)$. Boron has two isotopes—^{10}B with about 20% abundance and ^{11}B with about 80% abundance. This helped in identifying peaks. There is likely a peak at 44 due to $H^{11}BO_2$, but this was masked by the large CO_2 peak. The dimers of HBO_2 at 88-89 may be formed directly from the sample or induced by the free-jet expansion process. These results suggest $HBO_2(g)$ and/or $BO_2(g)$ are the major vapor species.

mass to charge	Probable ion	Probable parent	Intensity—900 C	Intensity—1000 C	Intensity—1100 C
43	$H^{10}BO_2^+$ or $^{11}BO_2^+$	$H^{10}BO_2$ or $^{11}BO_2$	0.10	0.40	0.96
46	NO_2^+	NO_2	n/o	0.06	0.08
62	$H_3{}^{11}BO_3^+$	$H_3{}^{11}BO_3$	0.08	0.05	n/o
88	$H_2{}^{11}B_2O_4^+$	$H_2{}^{11}B_2O_4$	n/o	0.05	0.05
89	$H_3{}^{11}B_2O_4^+$?	$H_3{}^{11}B_2O_4$?	n/o	0.04	n/o

Table III. Mass Spectrometer results for high density CVD BN with about 2% water vapor/oxygen. Intensities are in arbitrary units.

Using the thermodyamic vapor pressures of these species, we can calculate the linear rate constant, assuming gas transport through the boundary layer is rate limiting. The expression for a flat plate is (18):

$$J = 0.664\,(\mathrm{Re})^{0.5}\,(Sc)^{0.33}\,\rho(HBO)\,\frac{D}{L} \qquad (6)$$

$$\mathrm{Re} = \frac{\rho v L}{\nu} \qquad Sc = \frac{\nu}{\rho D}$$

Here Re and Sc are the Reynolds and Schmidt numbers, respectively. In these expressions, ρ is the concentration of oxygen, $\rho(HBO_2)$ is the density of HBO_2, v is the linear gas velocity taken as 1.56 cm/s, ν is the viscosity taken as 6.16 x 10^{-4}, L is a characteristic dimension taken as 0.5 cm, and D is the diffusitivity of $HBO_2(g)$. The vapor pressures of HBO_2 from the thermodynamic calculations for Figure 2(a) of this paper were used to calculate the density of HBO_2. The diffusivity of HBO_2 was estimated from the following expression (17):

$$D = \frac{2}{3}\left(\frac{k_b}{\pi}\right)^{3/2}\left(\frac{1}{2m_{O_2}} + \frac{1}{2m_{HBO_2}}\right)^{1/2}\frac{T^{3/2}}{P}\left(\frac{d_{O_2} + d_{HBO_2}}{2}\right)^{-2} \qquad (7)$$

Here k_b is Boltzmann's constant, m are the molecular weights, and d are the molecular diameters.

These expressions were used to calculate the linear rate constants listed in Table II for 900, 1000, and 1100°C. Calculations were not done at 1200°C because the free energy minimization at constant pressure predicted that all the water vapor was consumed, as discussed earlier. This indicated that the constant pressure-free energy minimization did not model our flowing gas system at 1200°C. However the calculations at 900, 1000, and 1100°C show remarkably good agreement with experiment (Table II). This supports the role of water vapor and $HBO_2(g)$ diffusion through the boundary layer being rate limiting.

Next consider the parabolic rate constants. These are listed in Table II in terms of weight gain and plotted in Figure 8 in units of thickness ($\mu m^2/hr$). The conversion is made from equation (1) and the density of B_2O_3, so that:

$$k_p\ (mg^2/cm^4\text{-}hr) \times 370 = k_p(\mu m^2/hr) \qquad (8)$$

Expressing k_p in terms of thickness allows comparison to rates for the common protective oxides—SiO_2 on SiC (19) and Al_2O_3 on NiAl (20). Note that these are several orders of magnitude slower, as expected since B_2O_3 is a liquid scale. The activation energy for BN oxidation to B_2O_3 is equal to (227 +/- 10) kJ/mol.

The determination of the exact rate controlling step for oxidation of this type of CVD material is beyond the scope of this paper. However some general remarks can be made. The parabolic kinetics suggest that some type of diffusion process is rate limiting. This would be either oxygen diffusion inward, boron diffusion outward, or nitrogen diffusion outward. We did an experiment with 10% O_2/Ar oxidation at 1100°C to try to ascertain which of these is rate controlling. The results are listed in Table II and are very close to those for 100% Ar. This may suggest that if oxygen is rate controlling, it diffuses as a charged specie, which gives a small fractional rate dependence on $P(O_2)$, depending on the defect chemistry. However, our activation energy is higher than that measured for the self-diffusion of oxygen in B_2O_3 of 137.2 kJ/mol (21). The lack of oxidation rate dependence on $P(O_2)$ may also suggest that B or N diffusion outward is rate controlling. An investigation of the combustion of solid boron suggests that at very high temperatures boron diffusion outward is rate controlling due to the high estimated solubility of boron in B_2O_3 (22). Further experiments on the oxidation rate dependence on oxygen and nitrogen need to be done. Marker experiments would also be useful, but are complicated by the liquid film.

III. **Low Density CVD BN**

A typical TGA trace for a low density CVD BN is shown in Figure 9. The observed kinetics contrast with the high density CVD BN—kinetics are more rapid and closer to linear than parabolic. A clear, glassy scale formed which

showed evidence of dripping. Figure 10 shows the solidified scale—a smooth, featureless glass with numerous cracks from cooling. Linear growth kinetics indicate a non-protective film and that the reaction of BN and oxygen is likely the rate controlling step.

The major difference between these two systems is density and crystallinity. It is likely that oxygen has more access to the rapidly oxidizing surfaces in these lower density BN materials. These observations are consistent with those of other investigators. Oda and Yoshio (7) have observed linear kinetics with hexagonal BN particles. Lavrenko and Aleexev (8) have observed linear kinetics with their graphite like BN in this temperature range.

Conclusions

The oxidation behavior of three types of boron nitrides—hot pressed, high density CVD and low density CVD—has been examined. The hot pressed material has randomly oriented grains and exhibits a clear orientation dependence, with the faces normal to the c axis oxidizing slowest. Two regions of linear kinetics are observed. The high density CVD BN is a dense material with a high degree of crystallinity and orientation along the c axis normal to the plate face. It oxidizes slowly, according to a parabolic rate law. The ~20 ppm of water vapor present in the gas stream created volatile $H_xB_yO_z(g)$ species simultaneous with the oxidation process and led to paralinear behavior. Lower density CVD BN showed rapid linear growth rates—very likely due to the lower crystallinity and lower density of this material.

Acknowledgments

It is a pleasure to acknowledge the extensive help of D. Humphrey, NYMA NASA Lewis Group in running the TGA. Helpful discussions with Dr. E. Opila are also appreciated.

References

1. A. Lipp, K. A. Schwetz, and K. Hunold, "Hexagonal Boron Nitride: Fabrication, Properties and Applications," J. European Ceram. Soc., **5** 3-9, 1989.

2. I. L. Zagyansky and G. V. Samsonov, "The Problem of the Oxidizability of Boron Nitride," J. Appl. Chem. USSR, **25** 629-630, 1952.

3. N. G. Coles, D. R. Glasson, and S. A. A. Jayaweera, "Formation and Reactivity of Nitrides III. Boron, Aluminum, and Silicon Nitrides," J. Appl. Chem. 19, 178-181 (1969).

4. M. D. Lyutaya, I. G. Chernysh, and O. A. Frenkel, "Chemical Properties of Nitrides of the A(III)B(V) Type," Soviet Powder Metallurgy, **6** [90], 503-508, 1970.

5. L. T. Podobeda, A. K. Tsapuk, and A. D. Buravov, "Oxidation of Boron Nitride under Nonisothermal Conditions," Soviet Powder Metallurgy, **9** [165], 44-47, 1976.

6. L. E. Pechentkovskaya and T. N. Nazarchuk, "Effect of Different Crystal Structures of Boron Nitride on its High-Temperature Stability in Oxygen," Soviet Powder Metallurgy, **7** [223], 83-86, 1981.

7. K. Oda and T. Yoshio, "Oxidation Kinetics of Hexagonal Boron Nitride Powder," J. Mat. Sci., **28** 6562-6566, 1993.

8. V. A. Lavrenko and A. F. Alexeev, "High-Temperature Oxidation of Boron Nitride," Ceram. Int., **12** 25-31 (1986).

9. C. G. Cofer and J. Economy, "Oxidative and Hydrolytic Stability of Boron Nitride—A New Approach to Improving the Oxidation Resistance of Carbonaceous Structures," Carbon, **33** [4] 389-395 (1995).

10. T. Matsuda, "Stability to Moisture for Chemically Vapour-Deposited Boron Nitride," J. Mat. Sci., **24** 2353-2358 (1989).

11. C. A. Stearns, F. J. Kohl, G. C. Fryburg, and R. A. Miller, "A High Pressure Modulated Molecular Beam Mass Spectrometric Sampling System," NASA TM 73720, 1977.

12. M. W. Chase, Jr., C. A. Davies, J. R. Downey, Jr., D. J. Frurip, R. A. MacDonald; and A. N. Syverud, JANAF Thermochemical Tables, Third Edition, American Chemical Society and American Physical Society, New York, 1986.

13. G. Eriksson and K. Hack, "ChemSage—A Computer Program for the Calculation of Complex Chemical Equilibria," Met. Trans., **21B** 1013-1023 (1990).

14. C. S. Tedmon, Jr., "The Effect of Oxide Volatilization on the Oxidation Kinetics of Cr and Fe-Cr Alloys," J. Electrochem. Soc. **113** [8] 766-768 (1966).

15. E. J. Opila and N. S. Jacobson, "SiO(g) Formation from SiC in Mixed Oxidizing—Reducing Gases," Oxid. Met. **44** [5/6] 527-544 (1995).

16. E. J. Opila and R. E. Hann, Jr., "Paralinear Oxidation of CVD SiC in Water Vapor," J. Amer. Ceram. Soc., **80** [1] 197-205 (1997).

17. D. R. Gaskell, An Introduction to Transport Phenomena in Materials Engineering, Macmillan, New York, 1992.

18. L. U. J. T. Ogbuji and E. J. Opila, "A Comparison of the Oxidation Kinetics of SiC and Si_3N_4," J. Electrochem. Soc. **142** [3], 925-930 (1995).

19. F. S. Pettit, "Oxidation Mechanisms for Nickel-Aluminum Alloys at Temperatures Between 900 and 1300°C," Trans. Met. Soc. AIME **239**, 1296-1305 (1967).

21. T. Taneki, T. Ito, and T. Yamaguchi, "Self Diffusion in a Glassformer Melt Oxygen Transport in Boron Trioxide," Z. Naturforschung **26A**, 2058-60 (1971).

22. Glassman, F. A. Williams, and P. Antaki, "A Physical and Chemical Interpretation of Boron Particle Combustion," Twentieth Symposium (International) on Combustion/The Combustion Institute, 2057-64 (1984).

Figure Captions

1. X-ray diffraction scans of hot pressed BN (dashed line), high density CVD BN (dotted line) and low density BN (solid line).

2. Equilibrium vapor pressures of major species over (a) B_2O_3 + 1 bar O_2 and (b) B_2O_3 + 1 bar O_2 + 20 ppm H_2O.

3. Oxidation kinetics for hot pressed BN at 900°C.

4. SEM photo and EDS of hot pressed BN after 20 hr of oxidation at 900°C showing preferential oxidation of BN grains.

5. Oxidation kinetics of high density CVD BN at 1100°C (a) Parabolic and(b) Paralinear. Note the fit to the paralinear kinetics.

6. SEM photo of CVD BN after 50 hrs of oxidation at 900°C.

7. Model paralinear plots (a) $k_p = 2.13 \times 10^{-2}$ mg^2/cm^4-hr, $k_l = -2 \times 10^{-2}$ mg/cm^2-hr and (b) $k_p = 2.13 \times 10^{-2}$ mg^2/cm^4-hr, $k_l = -2 \times 10^{-3}$ mg/cm^2-hr. The second plot is still paralinear, but reducing the linear weight loss rate makes it appear parabolic in the first 1000 hrs.

8. Arrehenius plot of parabolic rate constants of high density CVD BN. Also shown are parabolic rate constants for silica on SiC (18) and alumina on Ni-Al (19) for comparison.

9. Oxidation kinetics of low density CVD BN at 900°C.

10. SEM photo of surface low density CVD BN oxidized for 50 hrs at 900°C.

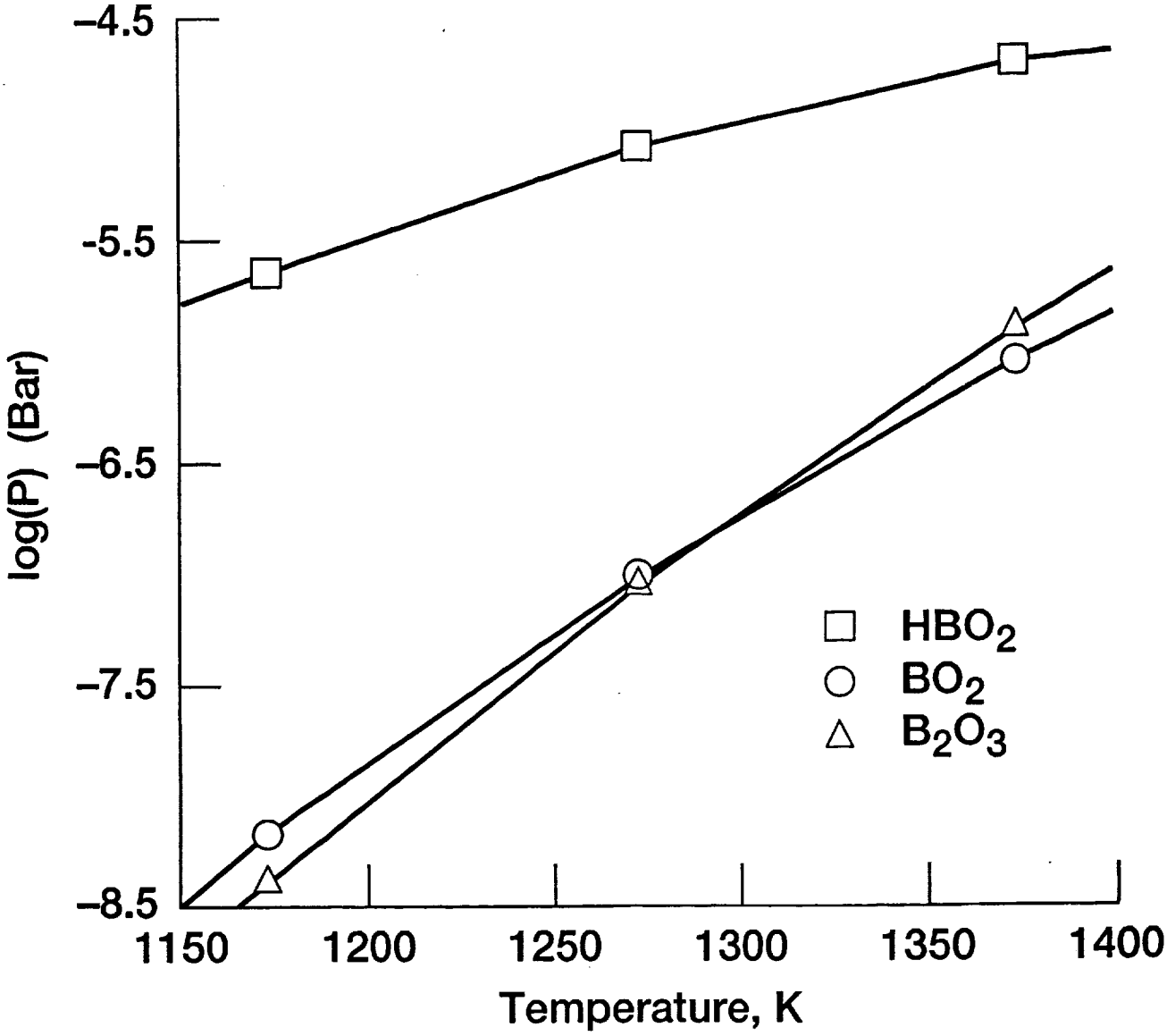
-4.5
-5.5
-6.5
-7.5
-8.5
log(P) (Bar)
1150
1200
1250
1300
1350
1400
Temperature, K
HBO2
BO2
B2O3

Figure 2

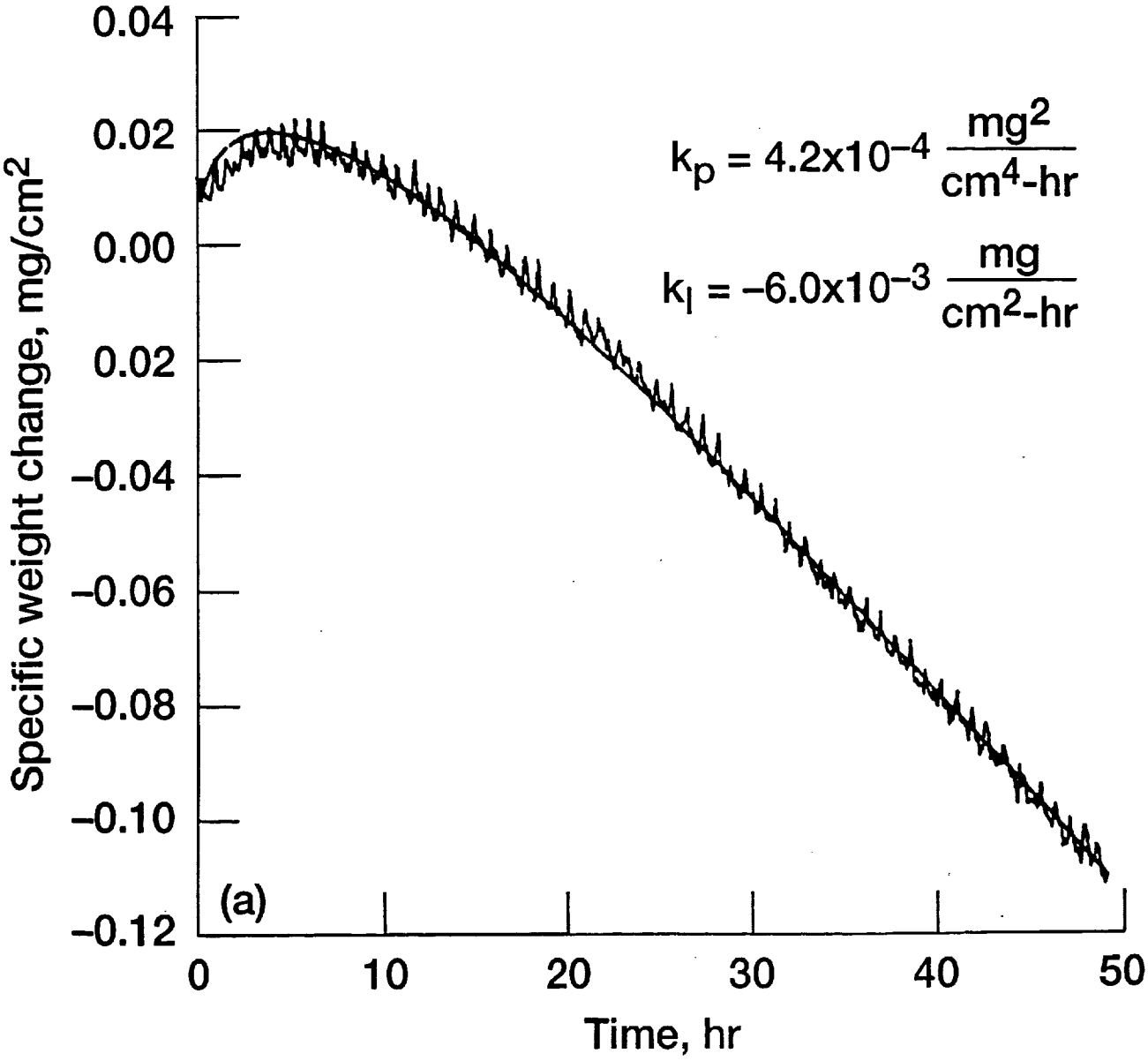
0.04
0.02
0.00
0.02
−0.04
−0.06
−0.08
−0.10
−0.12
Specific weight change, mg/cm²
$k_p = 4.2 \times 10^{-4} \frac{mg^2}{cm^4\text{-}hr}$
$k_l = -6.0 \times 10^{-3} \frac{mg}{cm^2\text{-}hr}$
(a)
0
10
20
30
40
50
Time, hr

Figure 5

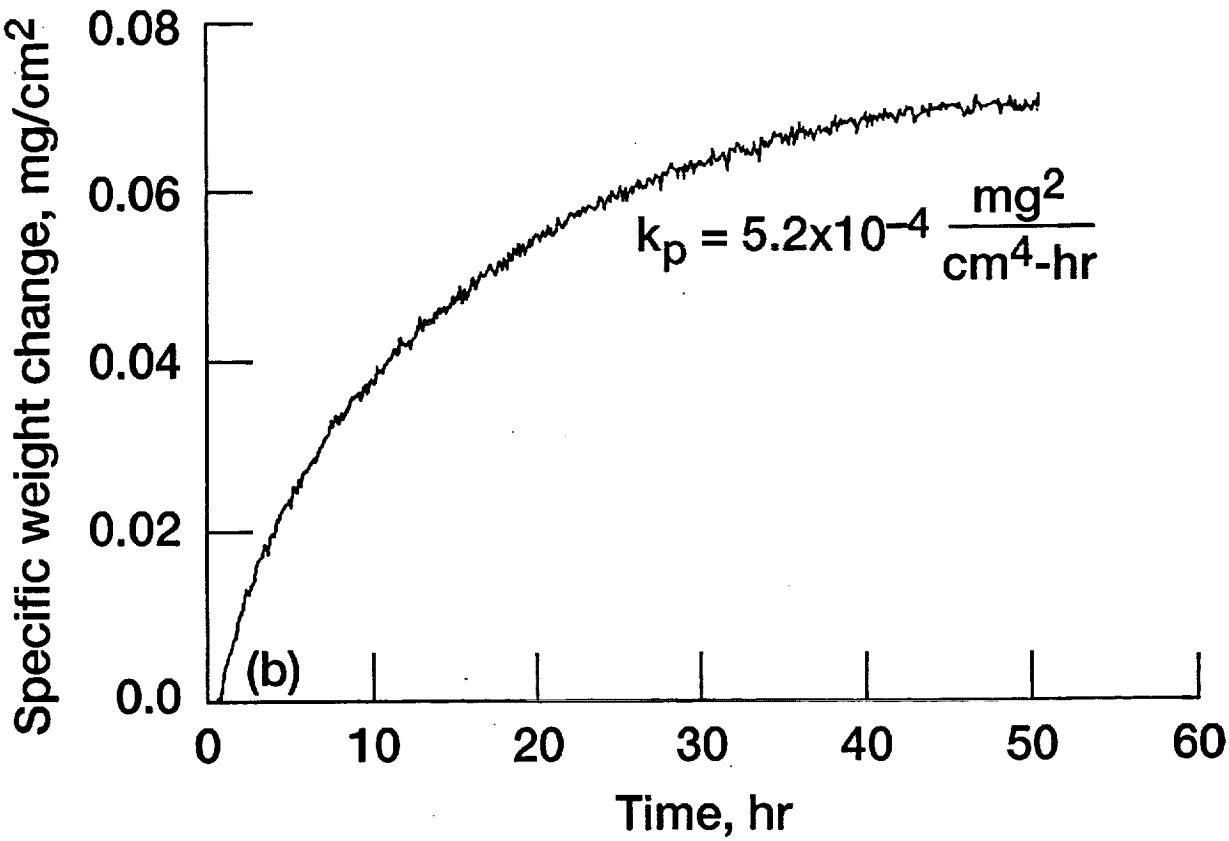
Specific weight change, mg/cm2
0.08
0.06
0.04
0.02
0.0
(b)
$k_p = 5.2 \times 10^{-4} \frac{mg^2}{cm^4\text{-}hr}$
0
10
20
30
40
50
60
Time, hr

Figure 5

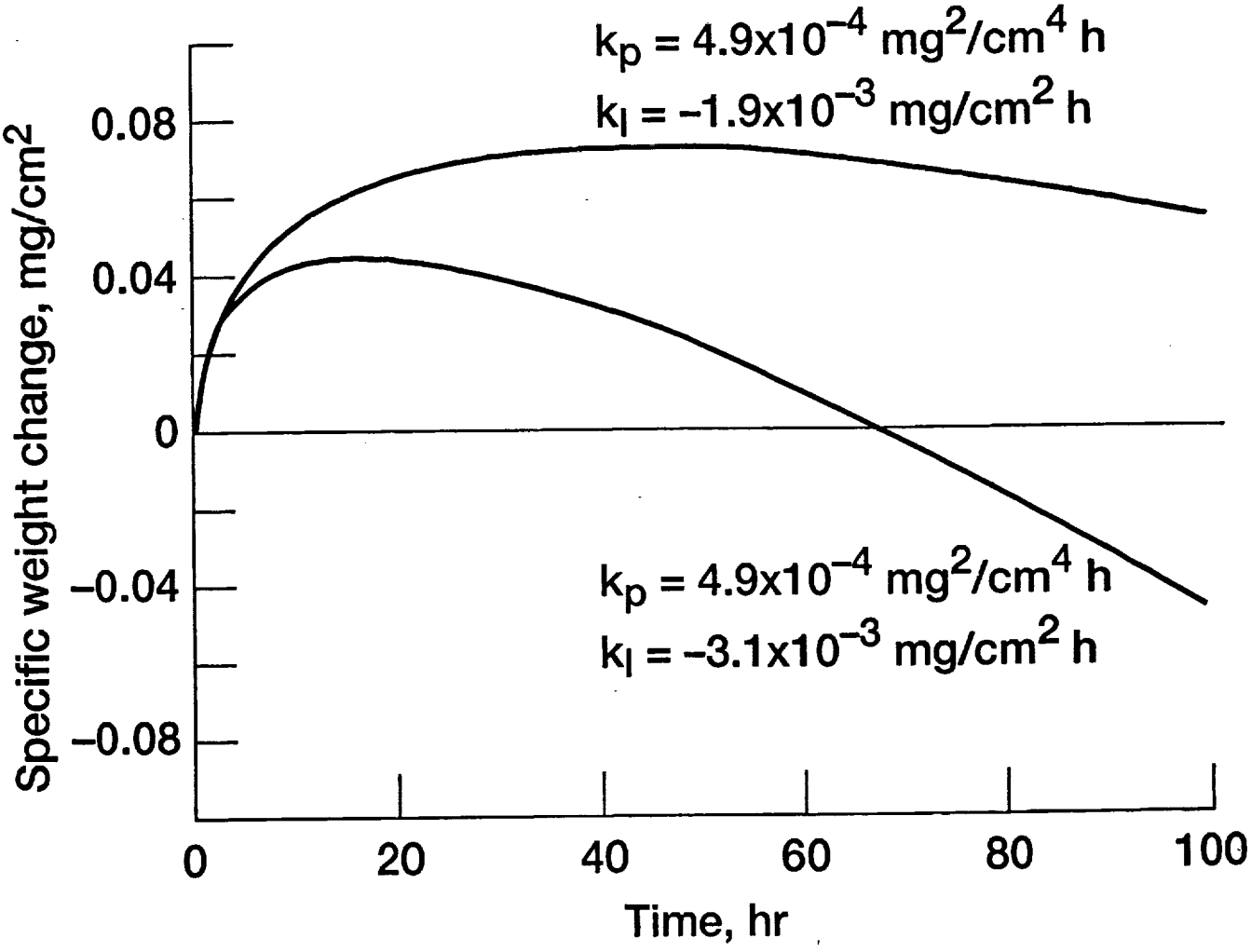
$k_p = 4.9x10^{-4}$ mg^2/cm^4 h
$k_l = -1.9x10^{-3}$ mg/cm^2 h
$k_p = 4.9x10^{-4}$ mg^2/cm^4 h
$k_l = -3.1x10^{-3}$ mg/cm^2 h
Specific weight change, mg/cm^2
0.08
0.04
0
−0.04
−0.08
0
20
40
60
80
100
Time, hr

Figure 7

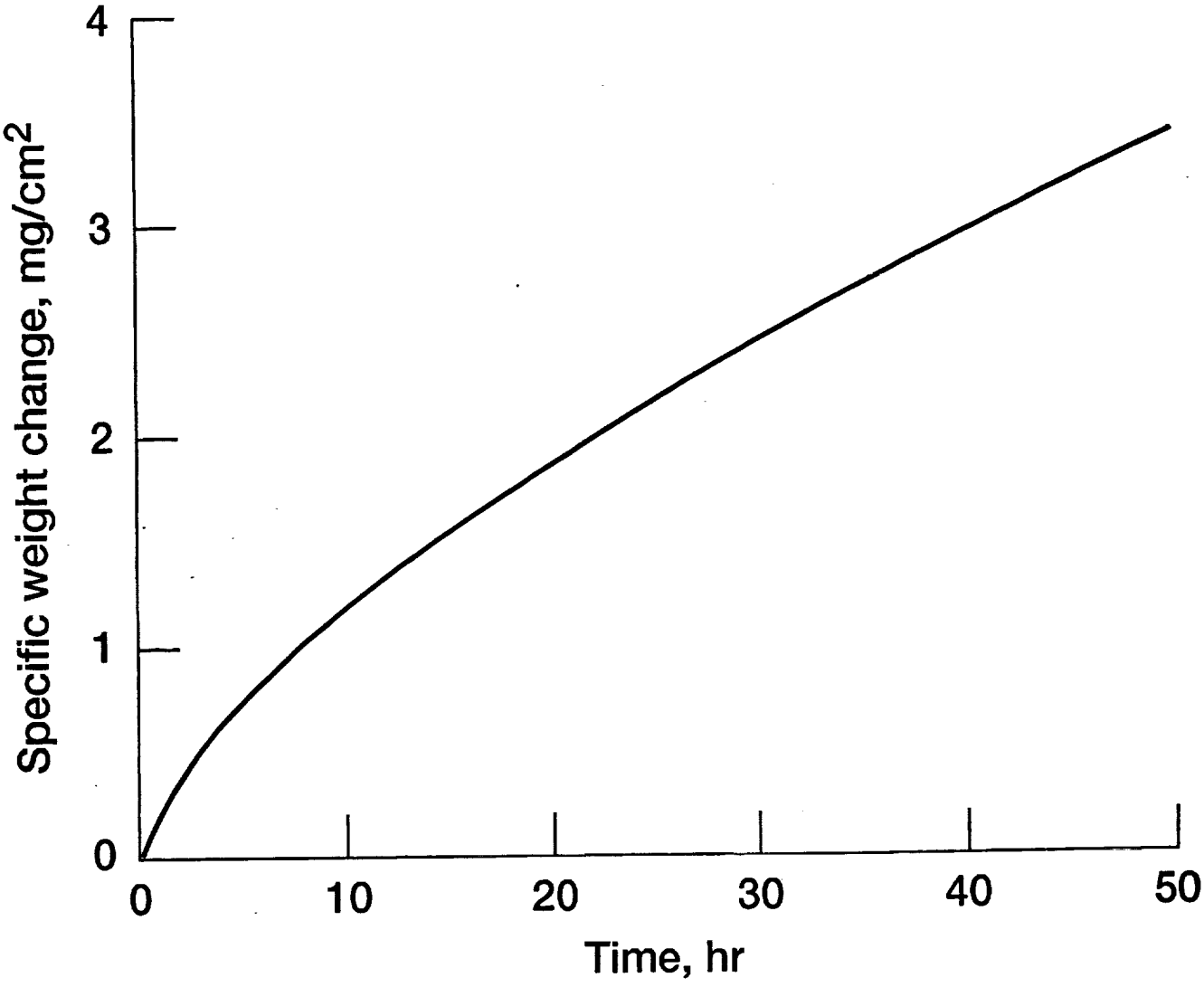

Figure 9